Fluorescence of rubidium in a submicrometer vapor cell: spectral resolution of atomic transitions between Zeeman sublevels in a moderate magnetic field

D. Sarkisyan, A. Papoyan, and T. Varzhapetyan

Institute for Physical Research, Armenian National Academy of Sciences, Ashtarak-2, 378410, Armenia

K. Blushs and M. Auzinsh

Department of Physics, University of Latvia, 19 Rainis Boulevard, Riga LV-1586, Latvia

Received April 6, 2004; accepted August 7, 2004; revised manuscript received August 23, 2004

It is experimentally demonstrated that use of an extremely thin cell (ETC) with the thickness of a Rb atomic vapor column of ~400 nm allows one to resolve a large number of individual transitions between Zeeman sublevels of the D_1 line of ^{87}Rb and ^{85}Rb in the sub-Doppler fluorescence excitation spectra in an external magnetic field of ~200 G. It is revealed that due to the peculiarities of the Zeeman effect for different hyperfine levels of Rb, all allowed transitions between magnetic sublevels can be clearly resolved for ^{87}Rb $F_g = 1 \rightarrow F_e = 1, 2$ and $F_g = 2 \rightarrow F_e = 1, 2$ fluorescence excitation. Also, relatively good spectral resolution can be achieved for ^{85}Rb $F_g = 2 \rightarrow F_e = 2, 3$ fluorescence excitation. Some partial resolution of transitions between magnetic sublevels is achieved for ^{85}Rb $F_g = 3 \rightarrow F_e = 2, 3$ fluorescence excitation. The spectral resolution of individual transitions allows one to easily observe both linear and nonlinear Zeeman effects in the fluorescence excitation spectra obtained with the help of the ETC. In the fluorescence spectra of a cell of usual length there is no evidence of a spectral resolution of individual transitions at $B \sim 200$ G. A simple magnetometer based on ETC with Rb with a submicrometer spatial resolution is described. © 2005 Optical Society of America

OCIS codes: 020.2930, 020.7490, 020.3690, 300.6210, 300.2530, 300.3700.

1. INTRODUCTION

Experimental realization of sub-Doppler spectroscopy of atomic vapors based on a thin cell with a column length $L \sim 10-1000$ μm has been reported in Refs. 1 and 2. However, revealing a sub-Doppler structure in transmission spectrum in this case requires a frequency modulation technique to be implemented for enhancement of the contrast of narrow resonances.[1,2] Nevertheless a simple laser-diode technique is sufficient to resolve spectrally atomic hyperfine transitions in alkali atoms because of use of extremely thin cells (ETCs) with $L \sim 100-600$ nm.[3,4] The sub-Doppler profile of the hyperfine transition in the case of the fluorescence excitation spectra in ETCs is narrower than that of transmission, and hence for some applications it is more convenient to use the fluorescence excitation spectrum.[3,4]

Recently it was demonstrated that the laser spectroscopy based on ETCs is a convenient tool to investigate the behavior of transitions between individual hyperfine states of Cs and Rb D_2 lines in a magnetic field of moderate strength. In these experiments a magnetic-field-induced, strong circular dichroism was observed.[5,6] However, because of the large number of magnetic sublevels and the numerous transitions allowed between individual pairs of magnetic sublevels for hyperfine transitions of Cs and Rb D_2 lines, it was impossible to spectrally resolve these transitions at a moderate strength of a magnetic field.

The aim of the present study is an experimental demonstration in which we attempt a complete resolution of the transitions between Zeeman sublevels in the fluorescence excitation spectrum and clarification of possible applications. To reach this aim a resonant D_1 transition in Rb was excited in ETCs placed in a moderate-strength magnetic field. Although saturation absorption spectroscopy provides narrower spectral lines, the advantage of the spectroscopy in ETCs is the absence of crossover resonances with large amplitudes. Moreover, substantial nonlinearity of the atomic response in SA and its strong dependence on the external conditions may strongly modify the spectrum in a magnetic field.

2. EXPERIMENTAL APPARATUS AND RESULTS

The experimental setup is presented in Fig. 1(a). The beam ($\varnothing$ 3 mm) of the wavelength $\lambda = 794$ nm, and the linewidth of 25 MHz from a single-frequency cw laser diode was directed at a normal incidence onto the ETC. The design of the ETC (which has garnet windows) is similar to one presented earlier.[3,4] As was shown in Refs. 7 and 8, the most narrow sub-Doppler linewidth of the hy-

perfine transition is achieved when the vapor column length $L = \lambda/2$. That was the reason why the thickness of an atomic vapor column of Rb was chosen to be $L = \lambda/2 \sim 400\,\text{nm}$. The column thickness L has been measured by the interferometric technique presented earlier.[7] The ETC operated with a specially designed oven with four openings: two openings for the laser beam transmission and two openings (orthogonal to the previous pair) for the side fluorescence detection. This geometry allows one to simultaneously detect fluorescence and transmission spectra. The fluorescence was detected by a photodiode with an aperture of $\sim 1\ \text{cm}^2$, which was placed at a 90° angle to the laser radiation propagation direction. The signal of the photodiode was recorded by a two-channel digital storage oscilloscope. The temperature T_{sa} of the sidearm of the ETC was kept at $\sim 120\,^{\circ}\text{C}$ (to prevent metal vapor condensation, the temperature of the windows was kept $\sim 10\,^{\circ}\text{C}$ higher). The sidearm temperature provides a vapor density of ^{85}Rb and ^{87}Rb of $N \sim 6 \times 10^{12}\,\text{cm}^{-3}$ and $1.5 \times 10^{13}\,\text{cm}^{-3}$, respectively.

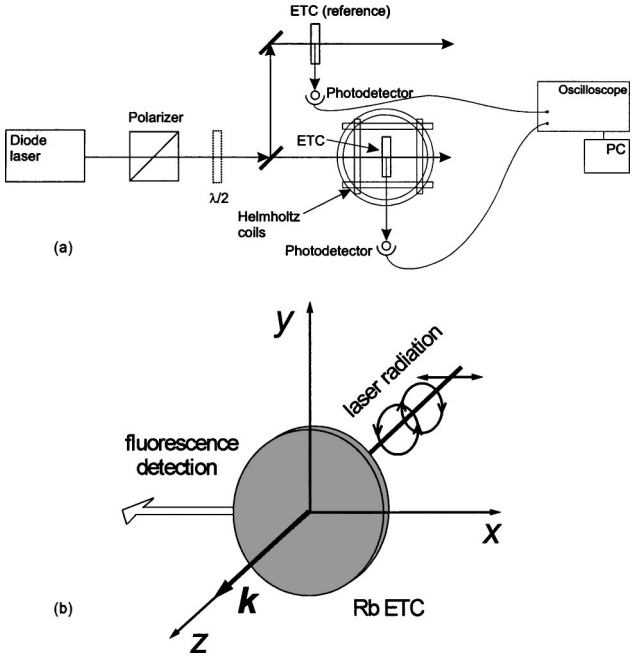

Fig. 1. (a) Schematic diagram of the experimental setup. (b) Geometric configuration of the experiment. The magnetic field is applied along the z or x axis.

The ETC was placed in the center of three pairs of mutually orthogonal Helmholtz coils, providing the possibility for us to apply a homogeneous magnetic field in an arbitrary direction. A Glan prism was used to purify the linear polarization of the laser-diode radiation; to produce a circular polarization, an antireflection-coated quarter-wave plate was utilized. The geometric configuration of the measurements is shown in Fig. 1(b).

A beam splitter directed 50% of the laser beam to the second ETC filled with Rb. The fluorescence signal from the second ETC has been used as a frequency and amplitude reference for $B = 0$ (light curves in Figs. 2–4).

It has been demonstrated that the linewidth of the fluorescence excitation spectrum in an ETC on the individual hyperfine transition could be approximately ten times

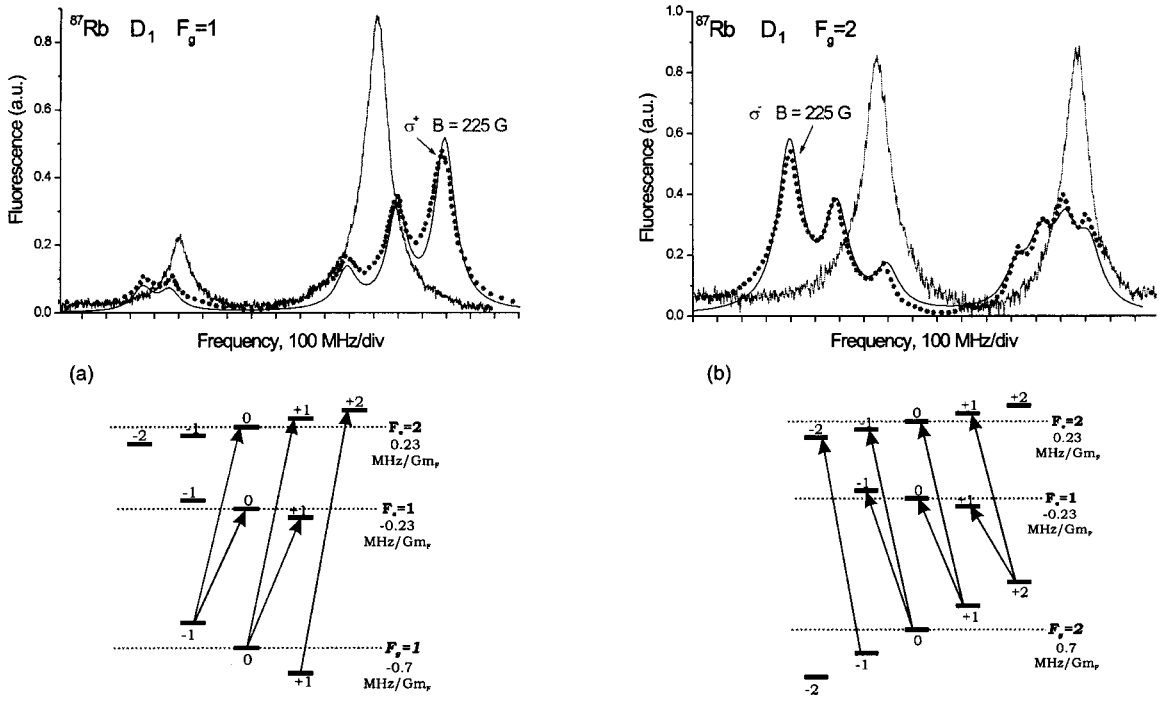

Fig. 2. Resonant fluorescence spectra on the D_1 line of ^{87}Rb with no magnetic field applied and in an external magnetic field $B = 225\,\text{G}$. (a) Transitions $F_g = 1 \rightarrow F_e = 1, 2$ with a σ^+ excitation; (b) transitions $F_g = 2 \rightarrow F_e = 1, 2$ with a σ^- excitation. Filled circles, experiment at $B = 225$ G; solid curve (nearly coinciding with experimental circles), numerical calculations for the case of $B = 225$ G; thick solid curve, reference spectra with no magnetic field applied ($B = 0$). The corresponding Zeeman sublevels and transitions (arrows) are shown in the lower diagrams.

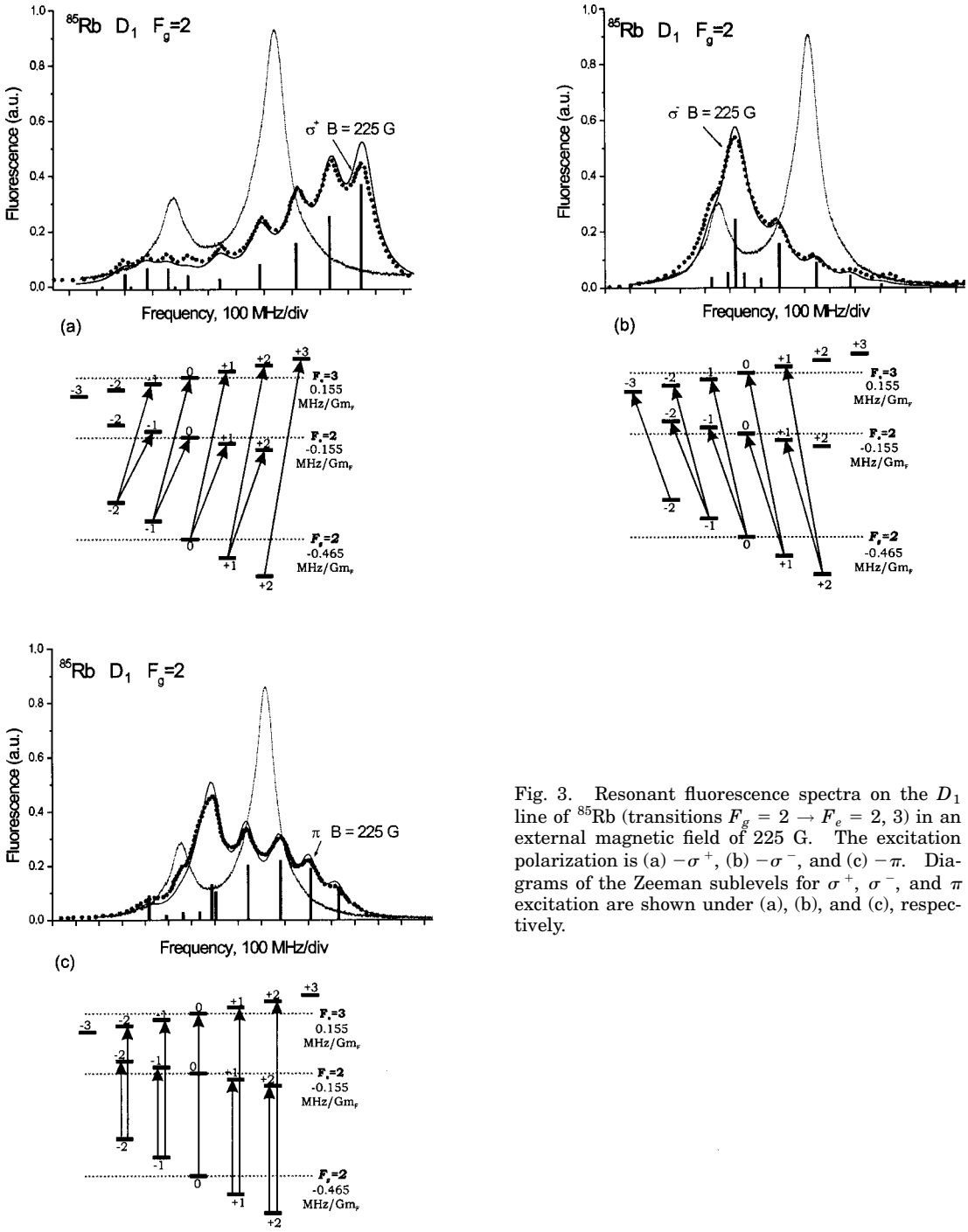

Fig. 3. Resonant fluorescence spectra on the D_1 line of ^{85}Rb (transitions $F_g = 2 \rightarrow F_e = 2, 3$) in an external magnetic field of 225 G. The excitation polarization is (a) $-\sigma^+$, (b) $-\sigma^-$, and (c) $-\pi$. Diagrams of the Zeeman sublevels for σ^+, σ^-, and π excitation are shown under (a), (b), and (c), respectively.

narrower than the Doppler linewidth,[3,4] and thus all the hyperfine transitions of the Rb D_1 line are resolved in the absence of the magnetic field ($B = 0$).

The fluorescence excitation spectra of ^{87}Rb in a longitudinal magnetic field $B = 225\,\mathrm{G}\,(\mathbf{B}\|\mathbf{k})$ with σ^+ excitation is presented in Fig. 2(a). It is easy to identify five peaks that correspond to the $F_g = 1 \rightarrow F_e = 1, 2$ components, in order of frequency increase [see Fig. 2(a), lower diagram]: $F_g = 1$, $m_F = -1,0 \rightarrow F_e = 1$, $m_F = 0, +1$, respectively, and $F_g = 1$, $m_F = -1,0,+1 \rightarrow F_e = 2$, $m_F = 0, +1, +2$, respectively. The fluorescence spectra of ^{87}Rb $F_g = 2 \rightarrow F_e = 1, 2$ in the case of longitudinal magnetic field $B = 225\,\mathrm{G}\,(\mathbf{B}\|\mathbf{k})$ with σ^- excitation is presented in Fig. 2(b). It is also easy to identify seven peaks that correspond to the atomic transitions presented in the diagram below Fig. 2(b) (for ^{87}Rb spectra excited in other configurations, see Ref. 9). The indicated values of the level shifts are given under the assumption of a linear Zeeman effect regime. This is for reference purposes only. It is not strictly valid for the strength of the magnetic fields used in this experiment.

The fluorescence spectra in the case of the longitudinal magnetic field $B = 225\,\mathrm{G}\,(\mathbf{B}\|\mathbf{k})$ with σ^+ and σ^- excitations for ^{85}Rb $F_g = 2 \rightarrow F_e = 2, 3$ are presented in Figs. 3(a) and 3(b). For the transversal magnetic field ($\mathbf{B}\|\mathbf{E}$) with π (linear) excitation, the fluorescence spectrum is

presented in Fig. 3(c). As can be seen, for σ^+ excitation there is a relatively good spectral resolution of each individual transition between Zeeman sublevels (nine resolved transitions). Relevant transitions between Zeeman sublevels are presented in the diagrams below Figs. 3(a), 3(b), and 3(c).

The nine resolved peaks in Fig. 3(a) correspond, in order of frequency increase, to the transitions $F_g = 2$, $m_F = -2, -1, 0, +1 \rightarrow F_e = 2$, $m_F = -1$, 0, $+1$, $+2$ (four peaks), respectively, and $F_g = 2$, $m_F = -2, -1, 0, +1, +2 \rightarrow F_e = 3$, $m_F = -1$, 0, $+1$, $+2$, $+3$ (five peaks), respectively. In the case of σ^- excitation and π (linear) excitation, the fluorescence spectra for $B = 225$ G presented in Figs. 3(b) and 3(c) demonstrate a partial overlapping of the transitions.

The fluorescence spectra in the case of the longitudinal magnetic field $B = 225$ G ($\mathbf{B} \| \mathbf{k}$) with σ^+ and σ^- excitations for ^{85}Rb $F_g = 3 \rightarrow F_e = 2$, 3 and for transversal magnetic field ($\mathbf{B} \| \mathbf{E}$) with π (linear) excitation are presented in Figs. 4(a)–4(c). Relevant transitions between the Zeeman sublevels are presented in the Fig. 4, lower part.

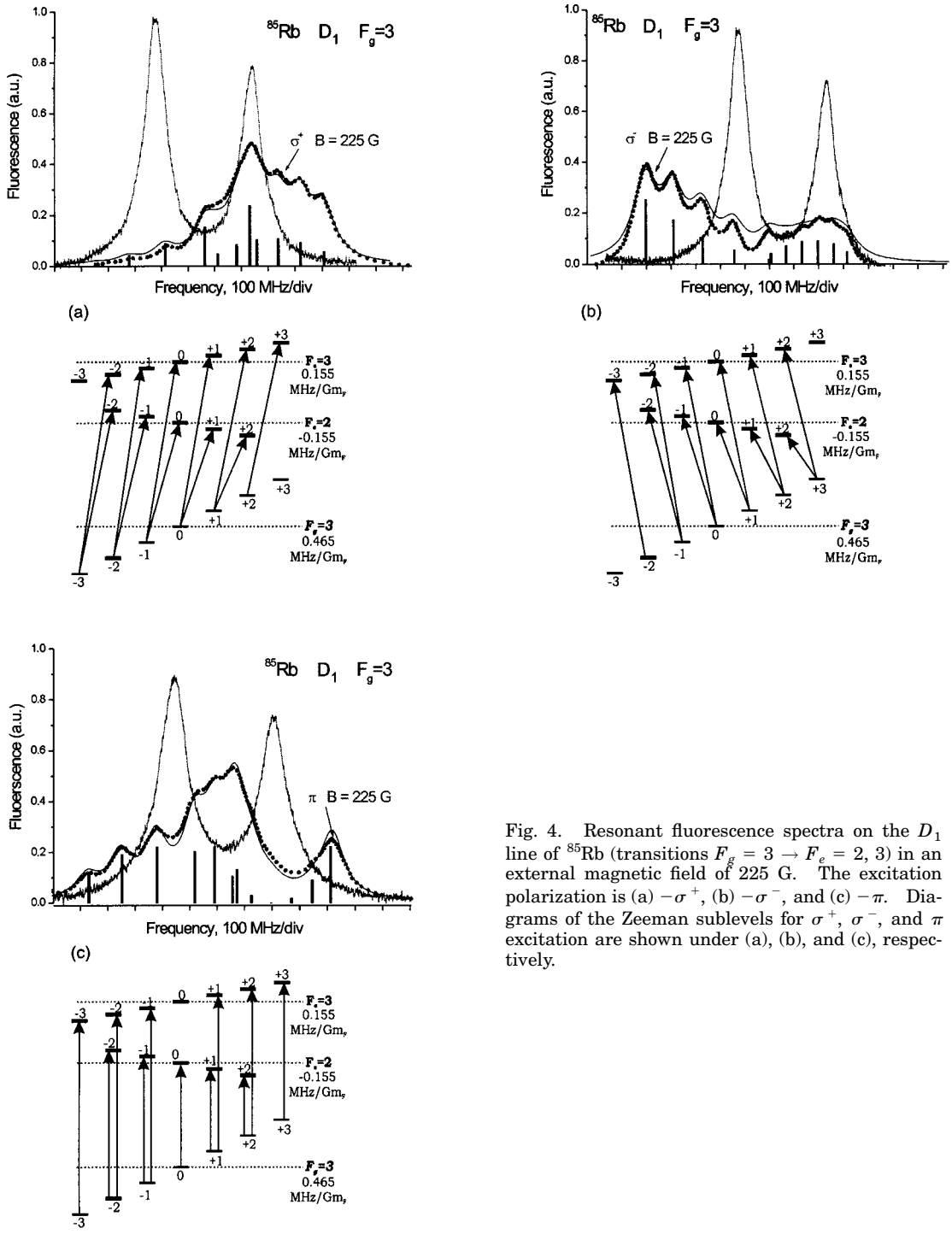

Fig. 4. Resonant fluorescence spectra on the D_1 line of ^{85}Rb (transitions $F_g = 3 \rightarrow F_e = 2$, 3) in an external magnetic field of 225 G. The excitation polarization is (a) $-\sigma^+$, (b) $-\sigma^-$, and (c) $-\pi$. Diagrams of the Zeeman sublevels for σ^+, σ^-, and π excitation are shown under (a), (b), and (c), respectively.

3. LASER-INDUCED FLUORESCENCE EXCITATION SPECTRA IN A MAGNETIC FIELD: SIGNAL SIMULATION

To simulate laser-induced fluorescence excitation (LIFE) spectra of Rb atoms in a magnetic field of intermediate strength, we use the following model. We assume that the laser radiation is weak and the absorption rate is small in comparison with the relaxation rates in the ground and excited states. This assumption is well justified by the observation of the LIFE spectrum independence on the laser intensity.

The Hamilton operator of the atom in a magnetic field can be written as

$$\hat{H} = \hat{H}_0 + \hat{H}_{\mathrm{HFS}} - \mu_J \cdot \mathbf{B} - \mu_I \cdot \mathbf{B}, \tag{1}$$

where $\hat{H}_0$ is a Hamiltonian operator of an unperturbed atom without taking into account nuclear spin and $\hat{H}_{\mathrm{HFS}}$ represents hyperfine interaction. The remaining two terms represent the interaction of the electronic magnetic moment μ_J of the atom and the nucleus magnetic moment μ_I with the external magnetic field $\mathbf{B}$. These magnetic moments are related to the respective electronic and spin angular moments $\mathbf{J}$ and $\mathbf{I}$ of the atom:

$$\mu_J = \frac{g_J \mu_B}{\hbar}\mathbf{J}, \qquad \mu_I = \frac{g_I \mu_0}{\hbar}\mathbf{I}, \tag{2}$$

where μ_B and μ_0 are the Bohr and nuclear magnetons, respectively, and g_J; g_I are electrotonic and nuclear Landé factors. The action of a magnetic field on the atom has two closely related effects. First, in the magnetic field, magnetic sublevels of the hyperfine levels are mixed by this field, giving rise to new atomic states, which are a linear combination of initial hyperfine levels:

$$|\gamma_k m\rangle = \sum_{F_e=|J_e-I|}^{F_e=J_e+I} C^{(e)}_{kF_e}(B, m)|F_e, m\rangle, \tag{3}$$

$$|\eta_s \mu\rangle = \sum_{F_g=|J_g-I|}^{F_g=J_g+I} C^{(g)}_{sF_g}(B, \mu)|F_g, \mu\rangle, \tag{4}$$

where $C^{(e)}_{kF_e}(B, m)$ and $C^{(g)}_{sF_g}(B, \mu)$ are mixing coefficients that depend on the field strength and the magnetic quantum number m and μ of the excited and ground state. The second effect is a deviation of the Zeeman magnetic sublevel splitting in the magnetic field for each hyperfine level from the linear one. It means that the additional energy of the magnetic sublevel obtained in the magnetic field is no longer linearly proportional to the field strength. For the D_1 transition four new atomic states $|\gamma_k m\rangle$ and $|\eta_s \mu\rangle$ are formed in the magnetic field for each isotope (two in the case of Rb atoms in the $5P_{1/2}$ state and two in the case of Rb atoms in the $5S_{1/2}$ state). As can be seen from Eq. (4), in the magnetic field the hyperfine angular-momentum quantum number F ceases to be a good quantum number, but magnetic quantum numbers m and μ are still good quantum numbers. This reflects the symmetry of the perturbation imposed by the magnetic field and means that only hyperfine sublevels with the same magnetic quantum numbers are mixed by the magnetic field.

The mixing coefficients $C^{(e)}_{kF_e}(B, m)$ and $C^{(g)}_{sF_g}(B, \mu)$ of the hyperfine states in the magnetic field and energies of these levels in the field ${}^{\gamma_k}E_m$, ${}^{\eta_s}E_\mu$ can be found as eigenvectors and eigenvalues of the Hamilton matrix [Eq. (1)]. In the case of two hyperfine levels, this problem has an analytical solution known as the Breit–Rabi formula (see, for example, Ref. 10).

The conditions of the experiment—diode-laser excitation in a stationary regime—allow us to use a relatively simple theoretical model for a LIFE spectrum simulation, namely, the so-called rate equations for Zeeman coherences (see Refs. 11–13 and a recent analysis of a relation of rate equations to optical Bloch equations for a density matrix[14]). As shown in Ref. 14, in the present conditions both approaches are equivalent. The configuration of the cell and the linear excitation regime (laser intensity below saturation) allow us, to a good approximation, to consider just one velocity group of atoms moving perpendicular to the laser beam and to neglect the effects of optical pumping, transition saturation, and reabsorption. The one-velocity-group approximation also means that we can consider near-resonant excitation of atoms—and this allows us to assume the laser line shape as Lorentzian. The Lorentzian is a good approximation of the center of the laser line. Considering the above assumptions, rate equations take the following form[14]:

$$\frac{\partial\, {}^{kl}f_{m_i m_j}}{\partial t} = -i\, {}^{kl}\omega_{m_i m_j}\, {}^{kl}f_{m_i m_j} - \Gamma\, {}^{kl}f_{m_i m_j} + \sum_{s\mu} \Gamma_p \langle \gamma_k m_i|\mathbf{d}\cdot\mathbf{e}|\eta_s\mu\rangle \times \langle \eta_s\mu|\mathbf{d}\cdot\mathbf{e}^*|\gamma_l m_j\rangle = 0, \tag{5}$$

$$\Gamma_p = \frac{|\epsilon_{\bar{\omega}}|^2}{\hbar^2} \frac{(\Gamma + \Delta\omega) + i({}^{ks}\omega_{m_i\mu} + {}^{sl}\omega_{\mu m_j})}{\left[\left(\frac{\Gamma}{2} + \frac{\Delta\omega}{2}\right) + i(\bar{\omega} + {}^{sl}\omega_{\mu m_j})\right]\left[\left(\frac{\Gamma}{2} + \frac{\Delta\omega}{2}\right) - i(\bar{\omega} - {}^{ks}\omega_{m_i\mu})\right]}, \tag{6}$$

where ${}^{kl}f_{m_i m_j}$ is an excited-state density matrix, ${}^{kl}\omega_{ij}$ denotes the Zeeman splitting $[{}^{kl}\omega_{ij} = ({}^{\gamma_k}E_i - {}^{\gamma_l}E_j)/(\hbar)]$, Γ is the total excited-state relaxation rate, $|\epsilon_{\bar{\omega}}|$ is the amplitude of the electric field of definite polarization $\mathbf{e}$, $\Delta\omega$ is

the laser linewidth (FWHM), and $\bar{\omega}$ is the central frequency of the laser spectrum. The transition dipole matrix elements of the type $\langle i|\mathbf{d}\cdot\mathbf{e}|j\rangle$ can be calculated with standard angular-momentum algebra.[15–17]

At each laser frequency a specific density matrix is calculated. Generally, the intensity of the fluorescence with a specific polarization $\mathbf{e}_{\text{obs}}$ in a transition between the excited γ_k and the final η_s state in the magnetic field can be calculated according to

$$I(\mathbf{e}_{\text{obs}}) = I_0 \sum_{mm'\mu} \sum_{kls} \langle \gamma_k m|\mathbf{e}_{\text{obs}}^* \cdot \mathbf{d}|\eta_s \mu\rangle \times \langle \gamma_l m'|\mathbf{e}_{\text{obs}}^* \cdot \mathbf{d}|\eta_s \mu\rangle^{kl} f_{mm'} \quad (7)$$

(see, for example Ref. 15). In this particular experiment, to have a LIFE spectrum we assume that, in the specific direction of observation, light with all polarization is detected (no analyzer in the detection system) and all possible transitions in fluorescence are observed (no spectral selection in the detection system). For this, Eq. (7) is averaged over all polarizations and final states of the transition.

This approach to spectrum calculation in the magnetic field and in absence of the field was used in the following simulation of experimentally observed signals.

4. DISCUSSION

Application of a magnetic field causes different energy shifts for different Zeeman sublevels, lifting the degeneracy; and pure nondegenerate atomic transitions can then be recorded. A simple analysis shows that the following conditions are favorable for this purpose: opposite signs of Landé factors g_F of the ground and the excited levels so that the transition frequency shift is enhanced, with g_F values as large as possible; a small value of F for the ground and the excited states to have fewer magnetic sublevels. Taking into account these conditions, the most convenient transition system is $^{87}\text{Rb}\,D_1\,F_g = 1, 2 \rightarrow F_e = 1, 2$. In fact, atomic transitions between the individual Zeeman sublevels in the ETCs on the $^{87}\text{Rb}\,D_1$ line have been observed already at $B \sim 50$ G; but for complete separation one needs to increase the field strength to $B \sim 200$ G (obviously use of a laser diode with a 1-MHz linewidth would somewhat improve the spectral resolution).

Vertical bars presented in Figs. 3 and 4 indicate the frequency position and the magnitude for individual transitions between the Zeeman sublevels obtained by numerical simulations with the model described above. As a result of our mixing the wave functions of different hyperfine states, we observe a nonlinear Zeeman effect for a number of sublevels, which results in the following consequences. For the transition $^{85}\text{Rb}\,F_g = 2,\ m_F = 0 \rightarrow F_e = 3,\ m_F = 0$ [Fig. 3(c), the eight vertical bar from the left] and for the transition $^{85}\text{Rb}\,F_g = 3,\ m_F = 0 \rightarrow F_e = 2,\ m_F = 0$ [Fig. 4(c), the third vertical bar from the left], the observed frequency shift is ~60 MHz (the case of π excitation). For a linear Zeeman regime the value of this shift is zero [see the diagrams for the case of π excitation below Figs. 3(c) and 4(c)]. Another consequence is the substantial modification of transition probabilities between different magnetic sublevels and the appearance of transitions that are strictly forbidden in the case of a weak magnetic field. As can be seen from Figs. 3 and 4, a number of new vertical bars with small amplitudes (which are different from the allowed transitions presented in the diagrams below Figs. 3, and 4) already exists at $B \sim 200$ G. Particularly, the peak value of the fluorescence on the transition $^{85}\text{Rb}\,F_g = 2,\ m_F = 0 \rightarrow F_e = 2,\ m_F = 0$ [Fig. 3(c)] and the peak value of the fluorescence on the transition $^{85}\text{Rb}\,F_g = 3,\ m_F = 0$

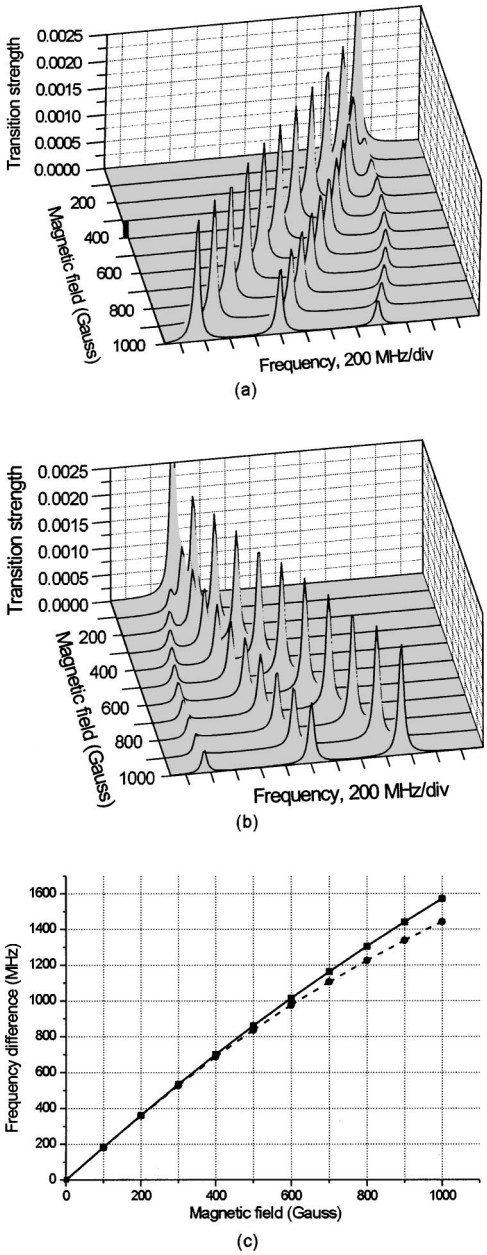

Fig. 5. Dependence of the transition strengths and the transition frequency positions on the magnetic field for (a) $^{87}\text{Rb}\,D_1\,F_g = 1 \rightarrow F_e = 2$ in the case of σ^+ excitation; (b) $^{87}\text{Rb}\,D_1\,F_g = 2 \rightarrow F_e = 1$ in the case of σ^- excitation; (c) magnetic field dependence of the frequency difference between the transitions $F_g = 1,\ m_F = +1 \rightarrow F_e = 2,\ m_F = +2$ and $F_g = 1,\ m_F = -1 \rightarrow F_e = 2,\ m_F = 0$ (σ^+ excitation, solid curve); $F_g = 2,\ m_F = 0 \rightarrow F_e = 1,\ m_F = -1$ and $F_g = 2,\ m_F = +2 \rightarrow F_e = 1,\ m_F = +1$ (σ^- excitation, dashed curve).

$\rightarrow F_e = 3, m_F = 0$ [Fig. 4(c)] has to be zero in the case of a linear Zeeman regime. Meanwhile, in Fig. 3(c) (the third vertical bar from the left) and in Fig. 4(c) (the ninth vertical bar mentioned in order of frequency increase) these peaks are distinctly observable as small vertical bars.

In Fig. 5(a) the results of numerical simulations of frequency position and transition strength are presented for $^{87}\mathrm{Rb}\, D_1 F_g = 1, m_F = -1, 0, +1 \rightarrow F_e = 2, m_F = 0, +1, +2$ transitions (σ^+ excitation) and for a magnetic field varying in the range of $B = 0-1000$ G. A similar plot is presented in Fig. 5(b) for $^{87}\mathrm{Rb}\, D_1 F_g = 2, m_F = +2, +1, 0 \rightarrow F_e = 1, m_F = +1, 0, -1$ transitions (σ^- excitation). Note that the frequency position of the first peak in Fig. 5(a) (transition $F_g = 1, m_F = +1 \rightarrow F_e = 2, m_F = +2$) has the highest frequency among all Zeeman transitions of the Rb D_1 line; and the frequency position of the last peak in Fig. 5(b), which corresponds to the transition $F_g = 2, m_F = +2 \rightarrow F_e = 1, m_F = +1$, has the lowest frequency among all Zeeman transitions of the Rb D_1 line.

The frequency shift between two side peaks for the magnetic field varying in the range of $B = 0-1000$ G is presented in Fig. 5(c) (solid curve is for $F_g = 1 \rightarrow F_e = 2$, and the dashed curve denotes $F_g = 2 \rightarrow F_e = 1$). As can be seen, the magnetic field sensitivity of the frequency depends on B, and it lays in the range of 1.6–1.9 MHz/G. The spectral peaks of individual Zeeman transitions are very well pronounced, and a precise measurement of the frequency shift between the two side peaks is possible. This may allow one to design a simple magnetometer for the B-field range of 50–1000 G with an unprecedented submicrometer spatial resolution. Although the magnetic field sensitivity of this magnetometer based on ETCs ($^{87}\mathrm{Rb}\, D_1 F_g = 1 \rightarrow F_e = 2$ system) will not be as high as the sensitivity of the magnetometers reported in Refs. 10 and 18, an important advantage could be gained for the measurement of strong (up to 1000 G) highly inhomogeneous magnetic fields with a strong spatial variation of strength.

It is important to note that in a cell of a usual length (1–10 cm), there is no evidence of a substructure at $B \sim 200$ G. To observe resolved Doppler-broadened transitions between the Zeeman sublevels in the absorption spectrum of a 1-cm-long Rb cell,[19] the magnetic field $B > 1000$ G was applied. In Ref. 20, to observe transitions between the Zeeman sublevels in a Cs cell of a usual length placed in a moderate magnetic field $B \sim 250$ G, the nondirect (selective reflection) process has been used.

5. CONCLUSION

We have demonstrated that use of ETCs with the thickness of Rb atomic vapor column $L \approx \lambda/2$ allows one to resolve spectrally a large number of individual transitions between Zeeman sublevels of the D_1 line of Rb in the sub-Doppler resonant fluorescence excitation spectrum in an external magnetic field of $B \sim 200$ G. The best spectral resolution is achieved for the transitions of $^{87}\mathrm{Rb}\, F_g = 1,2 \rightarrow F_e = 1, 2$ (all 12 Zeeman components are resolved), and this is caused by convenient parameters of the hyperfine levels. In a limited B-field range, a relatively good spectral resolution also could be achieved for $^{85}\mathrm{Rb}\, F_g = 2 \rightarrow F_e = 2, 3$ (nine resolved components). A partial resolution could be achieved for $^{85}\mathrm{Rb}\, F_g = 3 \rightarrow F_e = 2, 3$ (from 8 to 10 transitions out of 11 allowed components), whereas in a cell of a usual length (5–50 mm) there is no structure observed in a spectrum at $B \sim 200$ G.

The spectral resolution of transitions between Zeeman sublevels allows one to easily observe both linear and nonlinear Zeeman effects in the fluorescence spectra obtained with the help of ETCs.

Use of an ETC that is placed in a moderate magnetic field permits us to realize a pure (nondegenerate) atomic transition system on the Rb D_1 line. This technique, which provides a nice demonstration of the Zeeman effect by itself, could also be successfully applied for the D_1 lines of Cs, K, and other alkali metals.

The proposed ETC-based magnetometer scheme of the $^{87}\mathrm{Rb}\, D_1$ line, which allows for a submicrometer spatial resolution, might be of importance for the measurement of particular high spatial gradient magnetic fields ($B > 100$ G).

ACKNOWLEDGMENTS

The authors are grateful to A. Sarkisyan for his valuable participation in the development and fabrication of the ETC. This research was supported, in part, by the Armenian Ministry of Economics, grants 1351 and 1323.

Corresponding authors are David Sarkisyan (david@ipr.sci.am) and Marcis Auzinsh (mauzins@latnet.lv).

REFERENCES

1. S. Briaudeau, D. Bloch, and M. Ducloy, "Detection of slow atoms in laser spectroscopy of a thin vapor film," Europhys. Lett. **35**, 337–342 (1996).
2. S. Briaudeau, D. Bloch, and M. Ducloy, "Sub-Doppler spectroscopy in a thin film of resonant vapor," Phys. Rev. A **59**, 3723–3735 (1999).
3. D. Sarkisyan, D. Bloch, A. Papoyan, and M. Ducloy, "Sub-Doppler spectroscopy by submicron thin Cs-vapor layer," Opt. Commun. **200**, 201–208 (2001).
4. D. Sarkisyan, T. Becker, A. Papoyan, P. Thoumany, and H. Walther, "Sub-Doppler fluorescence on atomic D_2 line of sub-micron rubidium vapor layer," Appl. Phys. B **76**, 625–631 (2003).
5. A. Papoyan, D. Sarkisyan, K. Blush, M. Auzinsh, D. Bloch, and M. Ducloy, "Magnetic field-induced mixing of hyperfine states of the Cs 6 $^2P_{3/2}$ level observed with a submicron vapor cell," Laser Phys. **13**, 1–11 (2003).
6. D. Sarkisyan, A. Papoyan, T. Varzhapetyan, J. Alnis, K. Blush, and M. Auzinsh, "Sub-Doppler spectroscopy of Rb atoms on D_2 line in a sub-micron vapor cell in the presence of a magnetic field," J. Opt. **6**, S142–S150 (2004).
7. G. Dutier, A. Yarovitski, S. Saltiel, A. Papoyan, D. Sarkisyan, D. Bloch, and M. Ducloy, "Collapse and revival of a Dicke-type coherent narrowing in a sub-micron thick vapor cell transmission spectroscopy," Europhys. Lett. **63**, 35–41 (2003).
8. D. Sarkisyan, T. Varzhapetyan, A. Sarkisyan, Yu. Malakyan, A. Papoyan, D. Bloch, and M. Ducloy, "Spectroscopy in an extremely thin vapour cell: comparing the cell length dependence in fluorescence and in absorption tech-

niques," Phys. Rev. A **69**, 065802 (2004).
9. D. Sarkisyan, A. Papoyan, T. Varzhapetyan, K. Blush, and M. Auzinsh, "Zeeman effect on the hyperfine structure of the D_1 line of a submicron layer of ^{87}Rb vapor," Opt. Spectrosc. **96**, 328–334 (2004).
10. E. B. Aleksandrov, M. P. Chaika, and G. I. Khvostenko, *Interference of Atomic States* (Springer-Verlag, New York, 1993).
11. J. P. Barrat and C. Cohen-Tannoudji, "Etude du pompage optique dans le formalisme de la matrice densite," J. Phys. Radium **22**, 329,443 (1961).
12. C. Cohen-Tannoudji, "Atoms in strong resonant fields," in *Frontiers in Laser Spectroscopy* (North-Holland, Amsterdam, 1977).
13. M. P. Auzinsh and R. S. Ferber, "Optical-pumping of diatomic-molecules in the electronic ground-state—classical and quantum approaches," Phys. Rev. A **43**, 2374–2386 (1991).
14. K. Blush and M. Auzinsh, "Validity of rate equations for Zeeman coherences for analysis of nonlinear interactions of atoms with laser radiation," Phys. Rev. A **69**, 063806 (2004).
15. M. Auzinsh and R. Ferber, *Optical Polarization of Molecules* (Cambridge U. Press, Cambridge, UK, 1995).
16. R. N. Zare, *Angular Momentum* (Wiley, New York, 1988).
17. D. A. Varshalovich, A. N. Moskalev, and V. K. Khersonskii, *Quantum Theory of Angular Momentum* (World Scientific, Singapore, 1988).
18. D. Budker, W. Gawlik, D. Kimball, S. Rochester, V. Yaschuk, and A. Wies, "Resonant nonlinear magneto-optical effects in atoms," Rev. Mod. Phys. **74**, 1153–1201 (2002).
19. P. Tremblay, A. Michaud, M. Levesque, S. Thériault, M. Breton, J. Beaubien, and N. Cyr, "Absorption profiles of alkali-metal D lines in the presence of a static magnetic field," Phys. Rev. A **42**, 2766–2773 (1990).
20. N. Papageorgiou, A. Weis, V. A. Sautenkov, D. Bloch, and M. Ducloy, "High-resolution selective reflection spectroscopy in intermediate magnetic fields," Appl. Phys. B **59**, 123–126 (1994).